

Errata for the “THE MECHANICS OF METAMORPHIC FLUID EXPULSION”

1) As used in Equation 1, w is the volatile mass per unit volume of rock ($\sim 130 \text{ kg/m}^3$), not the weight fraction of volatiles as stated in the text. The error is not propagated through the text and the numeric value and units of the flux are correct.

2) The compaction time scale mentioned after Equation 4 overestimates the time scale for fluid expulsion in rocks that deform by power-law viscous creep, for rocks that deform according to

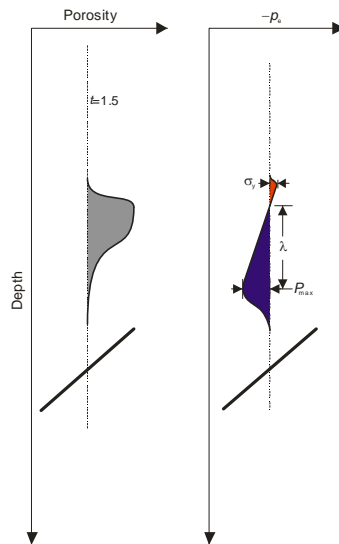
$$\dot{\epsilon} = A\Delta\sigma^{n_\sigma}$$

in response to uniaxially applied differential stress $\Delta\sigma$, a more accurate estimate of the time scale is

$$\tau = \frac{\delta}{v_0} = \frac{n_\sigma + 1}{\phi} \sqrt{\frac{\phi_0^{2n_\sigma - 2}}{c_\sigma A (q_0 \Delta \rho g)^{n_\sigma}}} = \frac{\phi_0^{n_\sigma - 1}}{\dot{\phi}}$$

where $c_\sigma = n_\sigma^{-n_\sigma} (3/2)^{n_\sigma + 1}$ (Connolly 2011). This scale differs from that given in the text by the factor $\phi_0^{n_\sigma - 1}$.

3) Figure 4, in the “compacting” limit the porosity distributions should not be symmetrical about the depth of the porosity maximum once the fluid pressure anomaly exceeds the yield stress (i.e., at $t > 1$). The symmetry is lost when the fluid pressure anomaly exceeds the yield stress because under these conditions the rate of dilational strain for a given effective stress magnitude is much larger for a negative effective stress than it is for a positive effective stress. To a first approximation (Connolly & Podladchikov 2000, 2007), this effect shrinks the vertical extent of the overpressured portion of the wave by a factor of $\sigma_y / (\delta \Delta \rho g)$ giving rise to the vertical porosity distribution illustrated below:



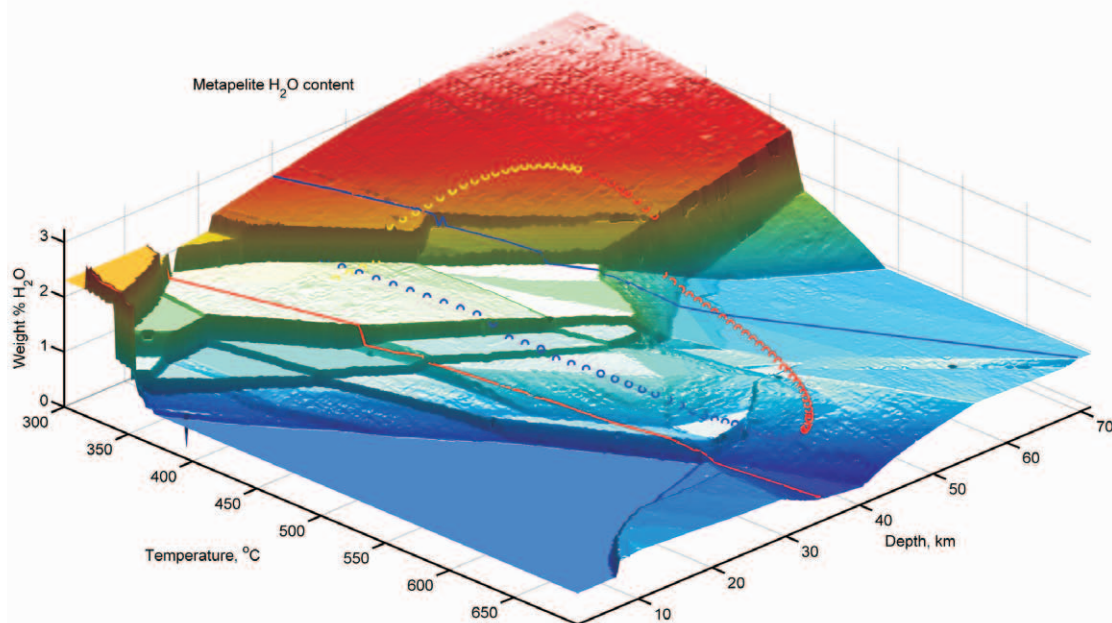


FIGURE 1 Water content of average pelitic sediment (Plank and Langmuir 1998) as a function of temperature and pressure, computed assuming equilibrium with a pure H₂O fluid. More than half the initial mineral-bound water content (7.6 wt%) is lost during diagenesis. The pelitic sediment contains 3 wt% CO₂, which is not accounted for in the model because decarbonation is sensitive to fluid–rock interaction (Ferry and Gerdes 1998; Connolly 2005). The red and blue lines indicate hot (20°C/km) and cold (10°C/km) metamorphic geotherms, respectively. The yellow-red-blue curve depicts the typical clockwise depth–temperature path followed by rocks during collision-belt metamorphism (England and Thompson 1984). The tectonically controlled, prograde, burial segment (yellow) is rapid (~1 My); thermal relaxation, in conjunction with isostatic rebound after burial (red) is slower (~10–100 My) and causes most prograde metamorphism; retrograde cooling (blue) does not affect the prograde mineral assemblage provided compaction isolates the rock from grain-scale interaction with fluids released by deeper metamorphism (Connolly and Thompson 1989). The increase in water content at temperature > 600°C is due to melting that occurs because the model assumes water saturation; this melting does not occur if the water released by low-temperature processes is expelled.

where κ represents thermal diffusivity ($\sim 10^{-6}$ m²/s for crustal rocks) and l_c represents crustal thickness. Thus a tectonic event that doubles crustal thickness to ~ 70 km is expected to generate metamorphism on a 100 My timescale. For an initial continental geotherm of $\sim 15^\circ\text{C}/\text{km}$, peak conditions of Barrovian metamorphism ($T \approx 600\text{--}700^\circ\text{C}$ at 20–30 km depth) imply heating rates of $\sim 3^\circ\text{C}/\text{My}$. In turn, these heating rates imply that metamorphic reaction fronts advance through the crust at ~ 200 m/My.

Assuming a heat conduction–controlled timescale and steady-state vertical fluid expulsion, average metamorphic fluid fluxes are:

$$q_m = -\frac{wl_c}{\rho_f \tau_m} = -\frac{w\kappa}{\rho_f l_c} \approx 10^{-12} \text{ m/s}, \quad (1)$$

where fluid density, ρ_f , is ~ 900 kg/m³, and volatile content, w , is ~ 0.06 kg_{volatile}/kg_{rock}. The timescale for metamorphism in subduction zones and continental rifting is significantly shorter, ~ 10 My, but the kinematics of these settings is such that the fluid fluxes are of the same order of magnitude as for collision belts (Connolly 1997a, 2005). Time-averaged flux estimates derived from field studies are also in this

range (Ferry and Gerdes 1998). In detail, variability of the devolatilization process is sufficient to assure that metamorphic fluid production occurs within horizons of intense reaction (Fig. 2) bounded by nonreacting rocks that presumably limit drainage. Equation (1) gives the time-averaged flux at the top of the metamorphic column, but unless all fluid production occurs at the base of the column, steady-state fluxes must be a strong function of depth (Fig. 2).

Petrologists periodically invoke advective heating by fluids (including melts) to explain anomalous heating relative to the classical model of England and Thompson (1984). The integrated fluid fluxes necessary to create significant thermal effects are comparable to the rock mass that is heated; thus it is implausible that such fluxes can be generated by the metamorphism itself unless fluid flow is focused (Connolly 1997b), but focused flow cannot explain pervasive heating. Thus, while heat advection models may prove correct, they leave open the troubling question of the flux source. Deficiencies in the England and Thompson model with regard to temperature (Lux et al. 1986) and exhumation (Amato et al. 1999) can be explained by mechanical effects, notably advective heating by the vertical displacement of blocks of crustal material and by both local and diffuse shear heating (Burg and Gerya 2005) without substantially changing the metamorphic timescale. Deficiencies with regard to rate are more problematic; most prominently, several lines of evidence suggest that the type section for Barrovian metamorphism evolved one to two orders of magnitude faster than predicted by the conductive timescale (Oliver et al. 2000; Ague and Baxter 2007). This evidence may ultimately require new models for regional metamorphism.

HYDRAULIC PROPERTIES: PERMEABILITY AND POROSITY

Although the hydraulic properties of metamorphic fluids are reasonably well known and not strongly variable (Walther and Orville 1982), the permeability and porosity of metamorphic rocks are poorly constrained. Indeed, it is conceivable that diagenetic processes eliminate all hydraulic connectivity prior to metamorphism. Discounting this possibility, the permeability of metamorphic systems

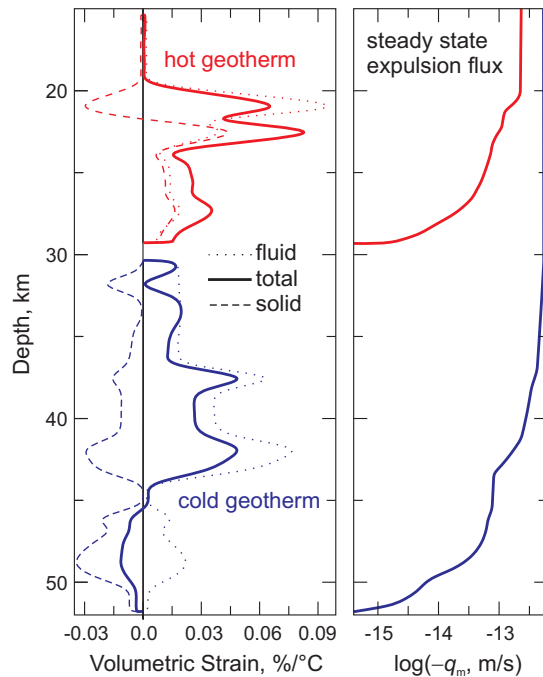


FIGURE 2 Devolatilization-induced, isobaric strain and steady-state fluid fluxes as a function of depth for the metamorphic model depicted in FIGURE 1. The strain is resolved into components resulting from fluid and solid production and corrected for the effect of thermal expansivity. For both hot and cold geotherms, fluid production occurs within restricted depth intervals. In the hot case, at depth > 23 km, solid volume increases during devolatilization and dilational deformation must create pore space for fluid release. Along the cold geotherm, solid densification creates much of the void space necessary to accommodate fluid production; in fact, in the lower 6 km of the section, the devolatilization-induced strain is negative; i.e. solid densification creates more void space than necessary to accommodate fluid. Fluid and solid production rates are the product of the corresponding component of the isobaric strain multiplied by the metamorphic heating rate. The fluid flux, q_m , is that which is necessary to drain the vertically integrated fluid production rate for a heating rate of 3°C/My. For the hot geotherm, the curves terminate at the onset of melting because the melting process is dependent on the dynamics of fluid expulsion.

is usually derived by estimating the metamorphic fluid flux and pressure gradient (Manning and Ingebritsen 1999). These estimates mask a dependence on the rate of metamorphism, which determines the fluid flux. This problem is avoided if the hydraulic regime is characterized by the flux necessary to maintain lithostatic fluid pressure rather than permeability. This flux, q_0 , defines a background state from which it is possible to assess the effect of local perturbations caused by devolatilization. Although this state is somewhat arbitrary, background fluxes are unlikely to exceed the average metamorphic fluid flux, which is dependent on the rate of metamorphism. Because the magnitude of the average flux decays with depth, it is reasonable to expect that the background flux has similar depth dependence. For quantitative illustration here, this dependence is ignored and q_0 is taken to be -10^{-13} m/s, a value comparable to the average flux expected in the upper half of a conductively heated metamorphic column (FIG. 2). The corresponding characteristic permeability, k_0 , is $\sim 10^{-20}$ m². While this permeability is low compared to permeabilities generally observed in situ in the upper crust (10^{-13} – 10^{-17} m², Ferry and Gerdes 1998; Manning and Ingebritsen 1999), it is unexceptional when compared to the permeabilities of argillaceous sediments (Neuzil 1994).

To a good approximation, the background flux is a proxy for all hydraulic properties of a metamorphic system except porosity. The term *porosity* here includes any interconnected fluid-filled voids present on spatial scales that are much smaller than the scale for fluid flow. Thus, porosity includes both grain-scale porosity generated by densification during devolatilization and small-scale fractures induced by the consequent dilational (i.e. volume changing) deformation. This porosity is critical to the dynamics of fluid expulsion because the hydraulic impact of metamorphic reactions is determined by how they influence permeability via porosity. Theoretical and empirical considerations indicate that permeability increases as the cubic or higher power of porosity (Norton and Knapp 1977; Neuzil 1994). This relationship implies that the percent-level porosities generated by devolatilization reactions lead to order of magnitude increases in the permeability of the reacted rocks provided initial porosities are small, i.e. $\ll 1\%$.

On the basis of isotopic diffusion profiles, Skelton et al. (2000) infer background porosities in the range $\phi_0 \approx 10^{-3}$ – 10^{-6} . These are consistent with grain-scale porosities of 10^{-3} – 10^{-6} measured in exhumed metamorphic rocks (Norton and Knapp 1977). An upper bound on premetamorphic porosities of $\sim 10^{-2}$ is provided by the sensitivity of geophysical measurements, which generally do not indicate fluids in the lower crust except in active metamorphic settings.

RHEOLOGY: THE BRITTLE-DUCTILE TRANSITION

Elevated fluid pressure is commonly attributed to compaction in the ductile lower crust. This association is tenuous because the classification of the crust into an upper brittle regime and a lower ductile regime is based on its response to tectonic stress, whereas compaction occurs in response to the difference between pore-fluid pressure and the mean stress. In fact, a compelling case can be made that the upper crust is characterized by hydrostatic pressures only because faulting maintains large-scale permeability (Zoback and Townend 2001). The absence of faulting in the aseismic lower crust allows processes, which include compaction but can also include retrograde metamorphism and diagenetic processes, to eliminate large-scale hydraulic structures. In the absence of such structures, the effective permeability of the crust would be limited by the vanishingly small permeability of argillaceous sediments (Neuzil 1994).

Regardless of the significance of the brittle-ductile transition for fluid pressure, as temperature increases, thermally activated time-dependent compaction must become important. Current experimental models for compaction are so uncertain that they provide no practical constraints (Farver and Yund 2000). Given this situation, an alternative is to calibrate ductile rheology in terms of the compaction timescale (τ_{B-D}), formally, the time required to decrease porosity by $\sim 36\%$ at the depth z_{B-D} (~ 15 km) and temperature T_{B-D} (~ 623 K) of the brittle-ductile transition. In this formulation, the coefficient of viscous creep is

$$\eta = \tau_{B-D} (\Delta\rho g z_{B-D})^n \exp\left(-\frac{Q}{RT} \frac{T - T_{B-D}}{T_{B-D}}\right), \quad (2)$$

where $\Delta\rho$ is the difference between rock and fluid density (~ 1900 kg/m³), n is the stress exponent, and Q represents the activation energy for viscous creep (~ 270 kJ/mol, with $n = 3$). From equation (2), for $\tau_{B-D} \approx 1$ My, the effective viscosity at the brittle-ductile transition is $\sim 10^{22}$ Pa·s and decays to $\sim 10^{14}$ Pa·s at 700°C.

THE COMPACTION SCALES

At near-lithostatic fluid pressures, the stress that causes compaction cannot be related directly to depth; rather, time-dependent compaction processes develop on a natural length scale known as the compaction length (McKenzie 1984). For crustal rheology (Connolly and Podladchikov 2004), the compaction length is

$$\delta = \sqrt[n+1]{\frac{\eta k_0}{\phi_0 \mu} \left(\frac{\phi_0}{\Delta \rho g} \right)^{n-1}}, \quad (3)$$

where μ represents fluid viscosity. In essence, δ is the length scale over which pore fluids can move independently of compaction processes; thus it is intuitive that δ increases with rock bulk strength, η/ϕ_0 , and the ease with which fluid can flow through rock, k_0/μ . Substituting equation (2) into equation (3), δ can be reformulated as

$$\delta = \sqrt[n+1]{\tau_{B-D} z_{B-D}^n |q_0| \phi_0^{n-2} \exp\left(-\frac{Q}{RT} \frac{T - T_{B-D}}{T_{B-D}}\right)}. \quad (4)$$

Equation (4) is relatively insensitive to the parameter estimates discussed previously, but δ is a strong function of temperature, decreasing from $\sim 10^4$ to ~ 1 m as temperature increases from 350 to 700°C. This suggests that at moderate temperatures, compaction is likely to influence metamorphic flow patterns on observable spatial scales. The compaction timescale for poorly drained rocks, $\tau_c \approx \eta/\phi_0/(\delta \Delta \rho g)^n$, is highly uncertain and only weakly related to the timescale for compaction at the brittle–ductile transition, τ_{B-D} , but its temperature dependence from equations (2) and (4) indicates that metamorphic temperature variations are sufficient to cause a 10-fold increase in compaction rates with depth.

THE LIMITING FLOW REGIMES

Although it is widely accepted that fluid expulsion occurs during metamorphism, it is not widely appreciated that this process is mechanical and as such strongly dependent on rheology. To illustrate this dependence, consider a minimal model for vertical flow in which (1) the fluid and rock are inelastic; (2) the rock compacts viscously if the difference between the fluid pressure, P_f , and rock pressure, P_r , is less than the tensile strength, σ_y (~ 5 MPa); and (3) the rock dilates plastically, i.e. hydrofractures, if $P_f - P_r > \sigma_y$. The model can be simplified further by discounting the volume

change associated with devolatilization. While this effect is often attributed mechanical importance, in poorly drained systems it is largely irrelevant (Connolly 1997a). Evidence for high fluid pressures during metamorphism requires that the metamorphic systems are poorly drained. Thus, the essence of devolatilization is to produce a permeable horizon surrounded by impermeable rocks through which negligible fluxes are sufficient to generate lithostatic fluid pressure. Within the reacting layer, even if devolatilization involves a net volume increase, fracturing maintains near-lithostatic conditions. Conservation of mass requires that in the absence of deformation the fluid flux must be equal to the drainage flux, q_0 , throughout the column. By Darcy's law, this flux is

$$q_0 = -\frac{k}{\mu} \left(\frac{\partial P_f}{\partial z} - \rho_f g \right), \quad (5)$$

if $\partial P_f/\partial z$ is the lithostatic gradient, $\sim \rho g$. However, within the reacted zone permeability, k , is much greater than the permeability, k_0 , of the overlying rocks. Therefore the last term in equation (5) must be small, which is only possible if $\partial P_f/\partial z$ is similar to the hydrostatic gradient, ρg , regardless of the near-lithostatic, absolute pressure. This situation gives rise to a positive effective pressure gradient, $\sim \Delta \rho g$, that causes deformation (FIG. 3).

The manner in which viscous compaction is superimposed on the foregoing scenario can be represented by the cases where the compaction timescale, τ_c , is much greater than, or comparable to, the metamorphic timescale, τ_m (FIG. 4). For a constant-volume devolatilization reaction, the mean fluid pressure within the rocks behind a reaction front is identical to the mean total pressure. Thus the upper and lower halves of the reacted interval are subject to negative (dilatational) and positive (compactive) effective pressures. If $\tau_c \gg \tau_m$, the rocks remain rigid on the timescale of reaction until the vertical extent of the reaction is large enough, i.e. $2\sigma_y/\Delta \rho g < \sim 500$ m, to cause micro- or macroscale fracturing at the top of the reacted rocks. Unless this produces fractures that breach the low-permeability barrier formed by the overlying rocks, fracturing acts as a homeostat that limits fluid pressure within the permeable zone as reaction progresses. Because the fracturing occurs at the top of the reacted rocks, the effect of continued reaction once the yield stress has been reached is to propagate fracture-generated porosity beyond the reaction front and decrease fluid

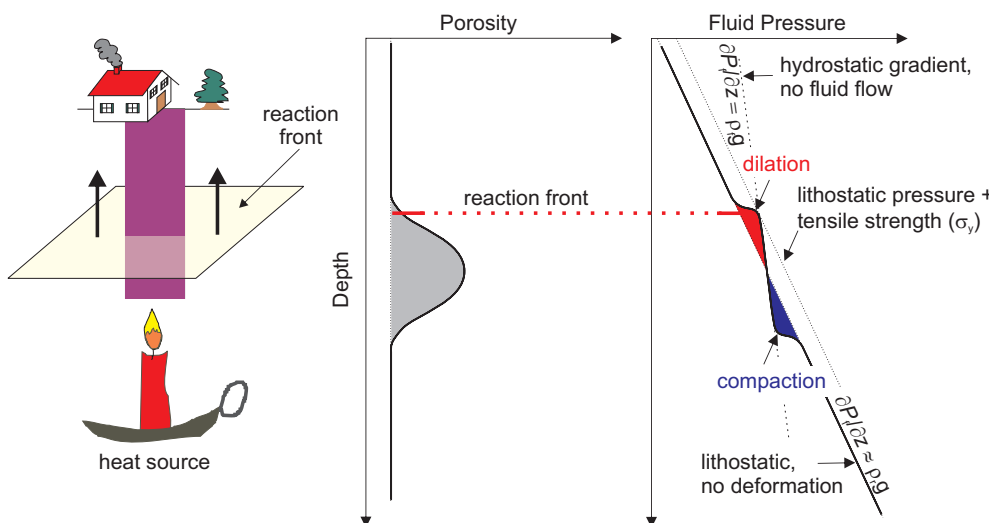


FIGURE 3 Conceptual model of metamorphic devolatilization. The reaction leaves a region of elevated porosity and permeability in its wake. Fluid flux is proportional to the permeability and the difference between the fluid pressure gradient and the hydrostatic gradient. In the absence of deformation, conservation of mass requires that this drainage flux must also be the flux within the reacted horizon with permeability $k \gg k_0$; this is possible only if the difference between the fluid pressure gradient and the hydrostatic gradient is small. However, this near-hydrostatic fluid-pressure gradient within the reacted rocks gives rise to an effective pressure, $P - P_r$, gradient of $\sim \Delta \rho g$, so that pore fluids become increasingly underpressured relative to the lithostat with depth within the high-porosity zone and, conversely, increasingly overpressured toward the reaction front. The resultant effective pressures are the driving force for deformation and fluid expulsion.

pressure. The propagation rate is dependent on the fracture mechanism, but because fracture permeability is also a cubic function of porosity (Norton and Knapp 1977), it is unlikely that the fracture front propagates much more rapidly than the reaction front. The important feature of this limiting scenario is that metamorphic reactions generate a permeable horizon that has the potential to allow lateral fluid flow.

In the compacting scenario ($\tau_c \approx \tau_m$), compaction squeezes fluid upward from the base of the reaction zone, while dilational processes at the top of the zone create porosity beyond the reaction front. If $\delta \Delta \rho g > \sigma_v$, this dilation can be accomplished by fracturing, but regardless of the dilational mechanism, the rate of dilation is limited by the rate at which devolatilization and compaction at depth supply the fluid that causes dilation. The combined effect of these processes is to propagate porosity upward relative to the reaction front. Because the rate of compaction at the base of the porous zone must increase with its vertical extent, compaction isolates the porous zone from the reaction front once the vertical extent of the reacted rocks is $\sim \delta$. The porosity then propagates upward independently of the reaction as a solitary wave. The essential features of this mode of fluid flow are that fluid pressures oscillate by approximately $\pm \delta \Delta \rho g$ about the lithostat and that fluid pressure gradients oscillate between hydrostatic and lithostatic. Since both τ_c and δ are proportional to rock shear viscosity, the classical picture of metamorphism as an isobaric process is recovered at high temperature when η is low, i.e. $\tau_c \ll \tau_m$ and $\delta \rightarrow 0$, but porosity waves slow and lengthen as they propagate upward into cool, upper crustal rocks (Connolly and Podladchikov 1998).

The primary effect of volume changes during devolatilization on the foregoing scenarios is to influence the mean fluid pressure within the reaction zone. Thus, the vertical extent of the reaction zone required to induce fracturing is smaller for a reaction with a positive isobaric volume change.

Compaction-driven fluid flow is widely appreciated in the context of both sedimentary basins and asthenospheric melt migration (Richter and McKenzie 1984; Connolly and Podladchikov 2000), and mathematical analysis has demonstrated that solitary porosity waves are a steady-state solution of the governing equations for fluid flow in compacting media (Barcilon and Lovera 1989). This analysis shows that the waves are stable provided the reaction-generated fluid flux is at least three times the flux that can be conducted through the unperturbed matrix, q_0 . When this condition is not met, the transient evolution at the reaction front is unchanged, but the waves dissipate as they propagate into the overlying matrix (Connolly and Podladchikov 1998). An additional requirement for the development of waves is that the vertical extent of the permeable source region must be $\sim \delta$. Both the localization of fluid production and the large resultant fluxes (FIG. 2) suggest that these requirements are met in metamorphic systems. Numerical analysis reveals that the one-dimensional waves just described decompose into elongate, tube-like waves in three dimensions (Connolly and Podladchikov 2007). Such waves, illustrated in the next section, do not substantially change the scales of compaction-driven fluid flow.

Chemical kinetic effects cause devolatilization at higher temperature than predicted by equilibrium models, but they do not fundamentally change the equilibrium picture because chemically limited rates are proportional to the free energy change, ΔG , of devolatilization (Jamtveit and Austrheim 2010). To a good approximation (Dahlen 1992),

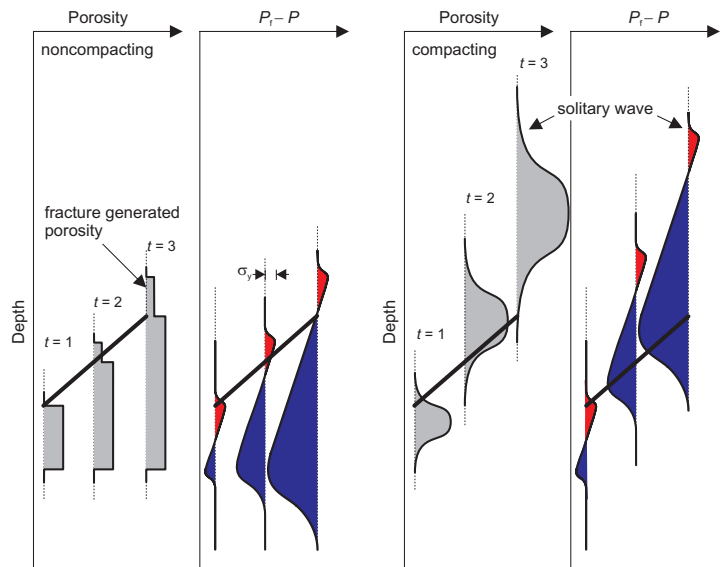


FIGURE 4 Time evolution of reaction-generated porosity and fluid overpressure, $P_t - P$, profiles for noncompacting and compacting scenarios. For each profile the baseline is indicated by a vertical dotted line. The baselines for the porosity and pressure profiles correspond to the background porosity, ϕ_0 , and lithostatic pressure. For simplicity, it is assumed that dilational deformation, in the form of microscopic or macroscopic fracturing, is instantaneous if fluid overpressure exceeds tensile strength (σ_t) (FIG. 3). The magnitude of the fluid-pressure anomaly within the reaction-generated porosity is proportional to the vertical extent of the high-porosity zone. Thus the anomaly grows as the reaction front advances upward until it becomes large enough to cause significant deformation. In the noncompacting case at $t = 1$, fluid pressure has just reached the failure condition. Thereafter failure acts as a homeostat requiring that any advance of the reaction front is accompanied by propagation of fracture porosity, an effect that lowers fluid pressure at the reaction front. Even in the unlikely event that such fractures should become self-propagating (Rubin 1998), they are not a mechanism for draining reaction-generated porosity. In the compacting scenario, compaction squeezes fluid upward, providing an independent mechanism for maintaining high fluid pressures that cause dilational deformation above the reaction front, an effect that ultimately propagates the porosity beyond the reaction front. Once this occurs ($t = 3$), the porous domain propagates independently of the reaction as a solitary wave of anomalous porosity (Richter and McKenzie 1984; Connolly 1997a).

ΔG is related to the displacement in temperature, ΔT , and fluid pressure, ΔP_t , from equilibrium conditions by

$$\Delta G = \Delta V \Delta P_t - \Delta S \Delta T, \quad (6)$$

where ΔS and ΔV represent the entropy and volume changes of devolatilization; typically $\Delta S = 3000\text{--}3500 \text{ J/}^\circ\text{C}$ and $\Delta V = -2 \cdot 10^{-5}$ to $+8 \cdot 10^{-4} \text{ J/Pa per kg}_{\text{volatiles}}$. These values imply that increasing temperature rapidly increases chemically limited kinetics until the process becomes heat-supply limited. A variation in fluid pressure must be greater than 5 MPa to have the same effect as a 1°C change in temperature; thus during prograde metamorphism, the effect of fluid pressure is to modulate the thermally controlled devolatilization rates (Connolly 1997a). For reactions with a positive isobaric volume change, rates decrease with decreasing fluid pressure and, counterintuitively, increasing fluid pressure increases the reaction rates.

LOOKING FOR LARGE LATERAL FLUXES

There is little doubt that lateral fluid flow occurs in metamorphic rocks (Ferry and Gerdes 1998). Both lithological contrasts and reaction-generated porosities give rise to permeable horizons that promote lateral fluid flow, but in overpressured systems, large lateral fluxes can only be explained by the existence of local drains into the perme-

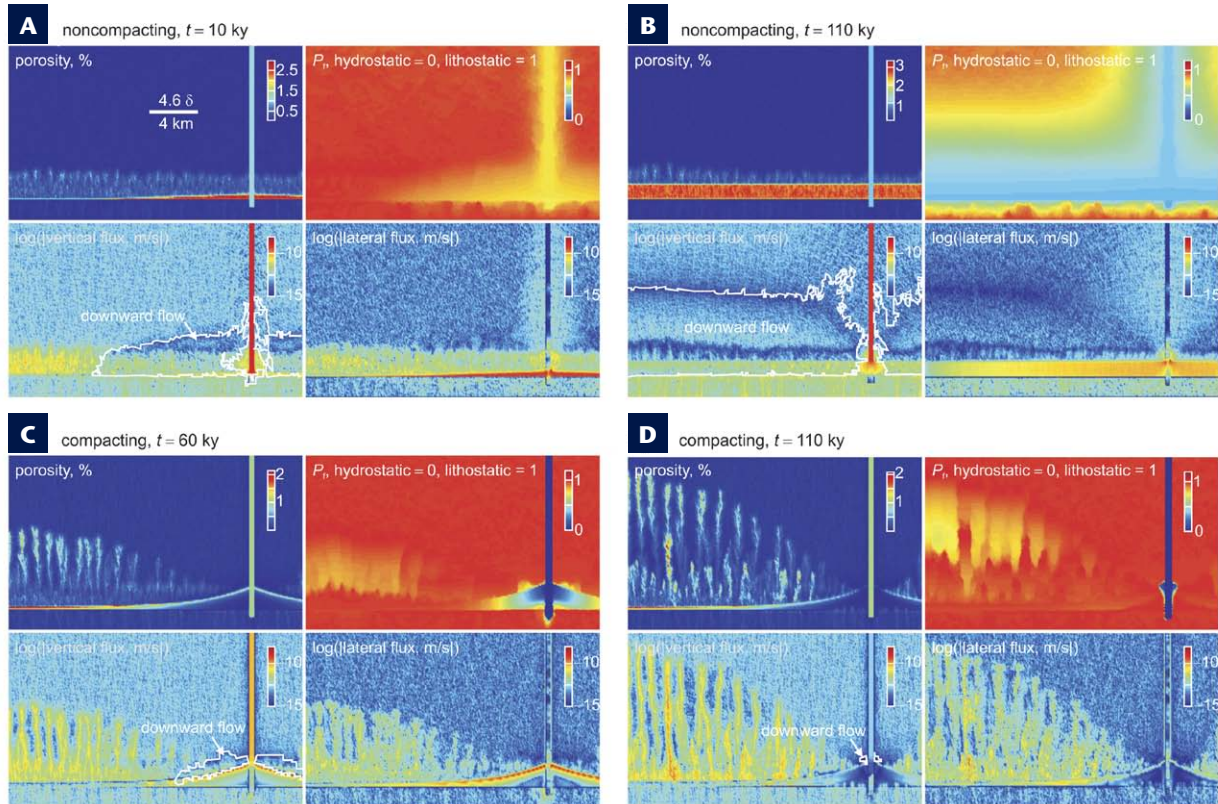


FIGURE 5 Numerical simulation of the influence of a permeable (10^{-17} m^2) shear zone on devolatilization-induced fluid flow for noncompacting (**A, B**) and compacting (**C, D**) scenarios. The plots of porosity, fluid pressure, and the magnitude of the vertical and horizontal components of the fluid flux are for a 24 km wide segment of the model spatial domain, which represents a $20 \times 40 \text{ km}$ crustal section. In the plots of vertical flux magnitude, large domains in which flow direction is predominantly downward are bounded by white curves; smaller domains of downward flow associated with individual porosity waves are not indicated. Prior to shear zone emplacement at $t = 0$, devolatilization proceeds for 100 ky, creating a $\sim 100 \text{ m}$ thick permeable horizon overlain by a fringe of fracture-generated porosity (as in Figure 4). At $t = 10 \text{ ky}$, both scenarios are virtually identical, the surge of fluid into the shear zone causes extraordinary fluid pressures and fluxes, and the consequent lowering of fluid pressure within the reacted horizon locally accelerates devolatilization. The noncompacting scenario rapidly reaches a quasi-steady state in which negligible pressure gradients are adequate to drain fluid from both within and about the reacted layer. In contrast, for the compacting scenario, by $t = 60 \text{ ky}$ the active portion of the reaction front is drained by tubelike porosity waves and is completely isolated from the shear zone. By $t = 110 \text{ ky}$, compaction has also eliminated the residual porosity in the inactive portion of the reaction zone; thus when dehydration resumes, the resulting flow is independent of the shear zone.

able upper crust. It is conceivable that ephemeral, brittle shear zones could function in this manner (Sibson 1992). Therefore, to illustrate the interplay between compaction and lateral flow, consider an initially poorly drained reaction front that is punctured by a high-permeability shear zone. To make the illustration less abstract, the fluid flow is modeled by solving the governing equations for compaction and heat flow numerically (Fig. 5). The details of this model are described elsewhere (Connolly 1997a), with the modifications here that the matrix is weakened during decompaction to simulate fracturing (Connolly and Podladchikov 2007) and random noise is added to the initial porosity to destabilize one-dimensional porosity waves (Fig. 4).

As anticipated by the one-dimensional scenario, in the noncompacting limit, a fringe of fracture-generated porosity develops above the reaction front (Fig. 5A), but

other than this feature, the model has no important nonkinematic behavior. With time, the reaction creates an ever thicker permeable layer that conducts the reaction-generated fluid, as well as fluids from the rocks above and below, to the fracture zone (Fig. 5B). The pressure gradient within the layer necessary to drive lateral flow is insignificant, with the consequence that the reaction front propagates uniformly upward. With time, such a model evolves toward a steady state, in which fluid pressures are hydrostatic above the reaction front and essentially all flow is focused into the shear zone. The flow pattern in this model is unsurprising, and the main conclusion to be drawn from it is that the pattern is determined by uncertain initial conditions and kinematics.

In the compacting scenario, the shear zone drainage is less effective because compaction throttles lateral fluid flow and the shear zone must compete with drainage by tubelike porosity waves. The waves (Fig. 5C) develop with a spacing comparable to the model compaction length ($\delta = 880 \text{ m}$), an effect that leads to focusing of reaction-generated fluxes. An unexpected feature of the flow pattern associated with the two-dimensional porosity waves is that the lateral and vertical fluxes are comparable. This convective pattern results because fluid is forced into the surrounding matrix by high pressures at the top of the wave and drawn back into the lower underpressured portion. This convective pattern is reminiscent of buoyancy-induced Rayleigh convection that develops in shallow hydrothermal systems (Norton and Knight 1977). However, dimensional analysis (Connolly 1997a) indicates that Rayleigh convection is unlikely in lower-crustal metamorphic settings, a conclusion also reached by more elaborate numerical modeling (Lyubetskaya and Ague 2009).

In the compacting model, drainage by the shear zone suppresses the development of porosity waves. The lateral extent of this near-instantaneous effect is quantitatively determined by the properties of the shear zone, but it decays rapidly as compaction seals the distal portions of

the layer. This decay accelerates with time as the shear zone becomes a more effective drain for the portion of the layer with which it is in hydraulic contact. In the numerical simulation, these effects seal the shear zone from the reaction front within 60 ky (Fig. 5c), and by 110 ky compaction has eliminated essentially all hydraulic contact with the shear zone (Fig. 5d). This latter effect has the consequence that subsequent devolatilization-induced fluid flow occurs independently of the shear zone.

DISCUSSION

Regional metamorphism occurs in an ambiguous rheological regime between the brittle upper crust and the ductile mantle. This ambiguous position has allowed two schools of thought to develop concerning the nature of metamorphic fluid flow. The classical school holds that metamorphic rocks are perfectly plastic, i.e., inviscid, and that any fluid generated by devolatilization is squeezed out of rocks as rapidly as it is produced (Walther and Orville 1982; Connolly and Thompson 1989; Yardley 2009). According to this school, permeability is a dynamic property and fluid flow is upward. In contrast, the modern school selectively uses concepts from upper-crustal hydrology that presume implicitly, if not explicitly, that rocks are rigid or, at most, brittle (Walder and Nur 1984; Manning and Ingebritsen 1999; Lyubetskaya and Ague 2009). For the modern school, the details of crustal permeability determine fluid flow, and because these details are poorly known, almost anything is possible.

Field studies offer some support to both schools. In particular, evidence of significant lateral fluid flow (Ferry and Gerdes 1998; Skelton et al. 2000) is consistent with flow in rigid media, while evidence for short (10^4 – 10^5 y), grain-scale fluid–rock interaction (van Haren et al. 1996; Graham et al. 1998; Ague and Baxter 2007) during much longer metamorphic events suggests that reaction-generated, grain-scale permeability is sealed rapidly by compaction, a phenomenon that is also essential to prevent extensive retrograde metamorphism. These observations provide a compelling argument for recognizing in conceptual models of fluid flow that metamorphic rocks are neither inviscid nor rigid, but have finite strength. The surprising consequence of this finite strength is that the steady-state solutions for fluid flow in porous, compacting media require

that fluid expulsion is channeled into waves of fluid-filled porosity. The waves develop on a characteristic length scale that is also the length scale for lateral fluid flow. In this context, porosity includes all hydraulically connected space present on a spatial scale $\ll \delta$. Thus, porosity waves may be manifest as self-propagating domains of fluid-filled fractures. Because δ is proportional to rock viscosity and consequently decreases exponentially with increasing temperature, the flow regimes of the classical and modern schools are recovered at high and low temperatures.

The compaction-driven flow regime has been illustrated here under the assumptions that compaction is time-dependent, that decompaction is largely time-independent, and that the far-field stress is isostatic. Near-surface sediments compact by time-independent plastic mechanisms that may well contribute to metamorphic porosity reduction. Fluid flow through porous media that compact dominantly by time-independent rheological mechanisms is also accomplished by porosity waves, but in contrast to the viscous case, the waves have no intrinsic length scale (Connolly and Podladchikov 1998; Miller et al. 2004). The assumption that decompaction occurs by fracturing is responsible for strongly channelized flow (Fig. 5). If fracturing is suppressed, porosity waves in viscous rocks are equant at high temperature but flatten as the waves propagate toward the surface (Connolly and Podladchikov 1998). Fluid flow in compacting media is in the direction of low mean stress. In nonisostatic systems, mean stress does not necessarily decay upward, an effect that could trap fluids beneath the tectonic brittle–ductile transition or draw fluids downward (Connolly and Podladchikov 2004). In the presence of far-field stress, the Mohr–Coulomb failure criterion implies that fracturing occurs at sublithostatic fluid pressures (Sibson 1992). This effect would reduce fluid pressures and influence fracture patterns but would not change the dynamics and scales of porosity waves limited by viscous compaction.


ACKNOWLEDGMENTS

Reviews and/or editorial suggestions by Craig Manning, Susan Stipp, Bjørn Jamtveit, Thomas Clark, Ingrid Aarnes, and George Hetenyi substantially improved this paper. This work was supported by Swiss National Science Foundation grants 200020-107889 and 200021-130411. ■

REFERENCES

- Ague JJ, Baxter EF (2007) Brief thermal pulses during mountain building recorded by Sr diffusion in apatite and multicomponent diffusion in garnet. *Earth and Planetary Science Letters* 261: 500-516
- Amato JM, Johnson CM, Baumgartner LP, Beard BL (1999) Rapid exhumation of the Zermatt–Saas ophiolite deduced from high-precision Sm–Nd and Rb–Sr geochronology. *Earth and Planetary Science Letters* 171: 425-438
- Barcilon V, Lovera OM (1989) Solitary waves in magma dynamics. *Journal of Fluid Mechanics* 204: 121-133
- Burg J-P, Gerya TV (2005) The role of viscous heating in Barrovian metamorphism of collisional orogens: thermomechanical models and application to the Lepontine Dome in the Central Alps. *Journal of Metamorphic Geology* 23: 75-95
- Connolly JAD (1997a) Devolatilization-generated fluid pressure and deformation-propagated fluid flow during prograde regional metamorphism. *Journal of Geophysical Research* 102(B8): 18149-18173
- Connolly JAD (1997b) Focused fluid movement in the middle crust: thermal consequences and silica transport. In: Jamtveit B, Yardley BWD (eds) *Fluid Flow and Transport in Rocks: Mechanisms and Effects*. Chapman Hall, London, pp 235-250
- Connolly JAD (2005) Computation of phase equilibria by linear programming: A tool for geodynamic modeling and its application to subduction zone decarbonation. *Earth and Planetary Science Letters* 236: 524-541
- Connolly JAD, Podladchikov YY (1998) Compaction-driven fluid flow in viscoelastic rock. *Geodinamica Acta* 11: 55-84
- Connolly JAD, Podladchikov YY (2000) Temperature-dependent viscoelastic compaction and compartmentalization in sedimentary basins. *Tectonophysics* 324: 137-168
- Connolly JAD, Podladchikov YY (2004) Fluid flow in compressive tectonic settings: Implications for midcrustal seismic reflectors and downward fluid migration. *Journal of Geophysical Research* 109: B04201, doi:10.1029/2003JB002822
- Connolly JAD, Podladchikov YY (2007) Decompaction weakening and channeling instability in ductile porous media: Implications for asthenospheric melt segregation. *Journal of Geophysical Research* 112: B10205, doi: 10.1029/2005jb004213
- Connolly JAD, Thompson AB (1989) Fluid and enthalpy production during regional metamorphism. *Contributions to Mineralogy and Petrology* 102: 347-366

- Dahlen FA (1992) Metamorphism of nonhydrostatically stressed rocks. *American Journal of Science* 292: 184-198
- England PC, Thompson AB (1984) Pressure-temperature-time paths of regional metamorphism 1. Heat transfer during the evolution of regions of thickened continental crust. *Journal of Petrology* 25: 894-928
- Etheridge MA, Wall VJ, Cox SF, Vernon RH (1984) High fluid pressures during regional metamorphism and deformation: Implications for mass transport and deformation mechanisms. *Journal of Geophysical Research* 89: 4344-4358
- Farver J, Yund R (2000) Silicon diffusion in a natural quartz aggregate: constraints on solution-transfer diffusion creep. *Tectonophysics* 325: 193-205
- Ferry JM, Gerdes ML (1998) Chemically reactive fluid flow during metamorphism. *Annual Review of Earth and Planetary Sciences* 26: 255-287
- Graham CM, Valley JW, Eiler JM, Wada H (1998) Timescales and mechanisms of fluid infiltration in a marble: an ion microprobe study. *Contributions to Mineralogy and Petrology* 132: 371-389
- Hetényi G, Cattin R, Brunet F, Bollinger L, Vergne J, Nábělek J, Diament M (2007) Density distribution of the India plate beneath the Tibetan plateau: Geophysical and petrological constraints on the kinetics of lower-crustal eclogitization. *Earth and Planetary Science Letters* 264: 226-244
- Holdaway MJ, Goodge JW (1990) Rock pressures vs. fluid pressure as a controlling influence on mineral stability – an example from New Mexico. *American Mineralogist* 75: 1043-1058
- Jamtveit B, Austrheim H (2010) Metamorphism: The role of fluids. *Elements* 6: 153-158
- Lux DR, DeYoreo JJ, Guidotti CV, Decker ER (1986) Role of plutonism in low-pressure metamorphic belt formation. *Nature* 323: 794-797
- Lyubetskaya T, Ague JJ (2009) Effect of metamorphic reactions on thermal evolution in collisional orogens. *Journal of Metamorphic Geology* 27: 579-600
- Manning CE, Ingebritsen SE (1999) Permeability of the continental crust: Implications of geothermal data and metamorphic systems. *Reviews of Geophysics* 37: 127-150
- McCuaig TC, Kerrich R (1998) *P-T-t*-deformation-fluid characteristics of lode gold deposits: evidence from alteration systematics. *Ore Geology Reviews* 12: 381-453
- McKenzie D (1984) The generation and compaction of partially molten rock. *Journal of Petrology* 25: 713-765
- Miller SA, Collettini C, Chiaraluce L, Cocco M, Barchi M, Kaus BJP (2004) Aftershocks driven by a high-pressure CO₂ source at depth. *Nature* 427: 724-727
- Neuzil CE (1994) How permeable are clays and shales? *Water Resources Research* 30: 145-150
- Norton D, Knapp R (1977) Transport phenomena in hydrothermal systems: nature of porosity. *American Journal of Science* 277: 913-936
- Norton D, Knight J (1977) Transport phenomena in hydrothermal systems: cooling plutons. *American Journal of Science* 277: 937-981
- Oliver GJH, Chen F, Buchwaldt R, Hegner E (2000) Fast tectonometamorphism and exhumation in the type area of the Barrovian and Buchan zones. *Geology* 28: 459-462
- Peng ZG, Vidale JE, Creager KC, Rubinstein JL, Gomberg J, Bodin P (2008) Strong tremor near Parkfield, CA, excited by the 2002 Denali Fault earthquake. *Geophysical Research Letters* 35: L23305, doi: 10.1029/2008GL036080
- Plank T, Langmuir CH (1998) The chemical composition of subducting sediment and its consequences for the crust and mantle. *Chemical Geology* 145: 325-394
- Richter FM, McKenzie D (1984) Dynamical models for melt segregation from a deformable rock matrix. *Journal of Geology* 92: 729-740
- Rubin AM (1998) Dike ascent in partially molten rock. *Journal of Geophysical Research* 103(B9): 20901-20919
- Scarpa R, Amoroso A, Crescentini L, Fischione C, Formisano LA, La Rocca M, Tronca F (2008) Slow earthquakes and low frequency tremor along the Apennines, Italy. *Annals of Geophysics* 51: 527-538
- Sibson RH (1992) Fault-valve behavior and the hydrostatic-lithostatic fluid pressure interface. *Earth-Science Reviews* 32: 141-144
- Skelton ADL, Valley JW, Graham CM, Bickle MJ, Fallick AE (2000) The correlation of reaction and isotope fronts and the mechanism of metamorphic fluid flow. *Contributions to Mineralogy and Petrology* 138: 364-375
- van Haren JLM, Ague JJ, Rye DM (1996) Oxygen isotope record of fluid infiltration and mass transfer during regional metamorphism of pelitic schist, Connecticut, USA. *Geochimica et Cosmochimica Acta* 60: 3487-3504
- Walder J, Nur A (1984) Porosity reduction and crustal pore pressure development. *Journal of Geophysical Research* 89(B13): 11539-11548
- Walther JV, Orville PM (1982) Volatile production and transport in regional metamorphism. *Contributions to Mineralogy and Petrology* 79: 252-257
- Yardley BWD (2009) The role of water in the evolution of the continental crust. *Journal of the Geological Society* 166: 585-600
- Zoback MD, Townend J (2001) Implications of hydrostatic pore pressures and high crustal strength for the deformation of intraplate lithosphere. *Tectonophysics* 336: 19-30 ■



What is the Lyell Collection?

Launched in 2007 to celebrate 200 years of the Geological Society of London, the Lyell Collection is an online collection comprising the Society's journal titles, Special Publications and key book series. Cutting edge science sits alongside important historical material, all captured and presented to the highest electronic standards and benefiting from the extensive functionality of HighWire Press' platform.

NEW DEVELOPMENTS FOR 2010:

Lyell Collection Complete (LCC): There will be no price increase for 2010, despite the addition of substantial new content and new titles.

Availability: From 2010 Lyell Collection subscriptions will be, by default, online-only. Subscribers wishing to receive print copies may do so by the payment of a 5% print surcharge. Online-only subscribers to the LCC may receive a print copy of all Special Publications by payment of £100/\$200.

Full archival access for all subscribers: The distinction between "Plus" and "Current" subscriptions will be discontinued – all subscribers will receive full archival access for their subscribed-to titles.

New titles: Three new titles will be added to the Lyell Collection at no additional charge to LCC subscribers:

- PGC** Petroleum Geology Conference series
- SIG** Scottish Journal of Geology
- PTGS** Proceedings of the Yorkshire Geological Society

Migration to H20: During 2010 all Lyell Collection titles will be migrated to HighWire Press' enhanced hosting platform.

Individual access to the Lyell Collection

Fellows of the Geological Society enjoy extensive access to Lyell Collection content, including:

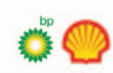
- JGS, QJEGH or GEEA online (including the full archive)
- The Historical Transactions of the Geological Society of London (1811-1856)
- The Books Archive (all Special Publications, Memoirs and Engineering Geology Special Publications published prior to the current and three previous calendar years)
- The option to access all current titles via the Full Book Collection

To find out more about becoming a Fellow visit www.geolsoc.org.uk/join

Library access to the Lyell Collection

Access to the full content of the Lyell Collection is via a range of subscription options, or pay-per-view. Additional content added for the 2010 subscription year is included in Lyell Collection Complete Subscriptions.

To order the Lyell Collection or individual journal titles, or request further information or a free trial, please contact:

<ul style="list-style-type: none"> ● In UK and Europe: Email: geologicalsociety@accucoms.com Telephone: +31 71 524 7630 Fax: +31 71 528 0628 ● In USA and Canada: Email: geologicalsociety@pcgplus.com Telephone: +1 617 395 4065 Fax: +1 617 354 6875 ● All other regions: Email: sales@geolsoc.org.uk Telephone: +44 (0)1225 445046 Fax: +44 (0)1225 442836 	<p>Web: www.accucoms.com</p> <p>Web: www.pcgplus.com</p> <p>Web: www.geolsoc.org.uk</p>	
---	--	---

Lyell Collection For more information visit www.geolsoc.org.uk/LyellCollection